Available online at www.sciencedirect.com
SCIENCE DIRECT®
Journal of Membrane Science 255 (2005) 157–165
journal of MEMBRANE SCIENCE
www.elsevier.com/locate/memsci

The role of adsorption on nanofiltration of azo dyes

Arlindo Caniço Gomes [a], Isolina Cabral Gonçalves [a,*], Maria Norberta de Pinho [b]

[a] *Department of Chemistry, Textile and Paper Materials Unit, University of Beira Interior, Rua Marquês d'Ávila e Bolama, 6201-001 Covilhã, Portugal*
[b] *Department of Chemical Engineering, Instituto Superior Técnico, Av Rovisco Pais 1, 1049-001 Lisboa, Portugal*

Received 24 September 2004; received in revised form 24 January 2005; accepted 25 January 2005
Available online 9 March 2005

Abstract

The influence of osmotic pressure and solute adsorption on permeate flux during nanofiltration (NF) of a wool textile dye solution was investigated. Solutions of C.I. Acid Orange 7 with concentrations ranging from 2 to 2000 mg/l were subjected to nanofiltration with a NF 45 membrane. An increase of flux decline with dye concentration was observed. The resistance-in-series model gives evidence that the main factor causing this flux decline is the solute adsorption. This is reinforced by the increase in the apparent rejection with dye concentration. Although osmotic pressure was taken into account, its contribution to a decrease of the driving force seems not to be significant. Adsorption resistance was calculated from a correlation between the pure water fluxes, measured before and after the essays, and feed dye concentration. A Langmuir isotherm type curve agreed well with experimental data. From the solution-diffusion model, the intrinsic rejection coefficient can be predicted as function of feed dye concentration.

Keywords: Textile industry; Nanofiltration; Solution-diffusion model; Azo dyes; Adsorption

1. Introduction

Wastewaters from textile industry are the main source of industrial pollution in several regions of Portugal. Dyes from dyeing operations are the major source of colour in textile effluents. In typical dyeing processes, 50–95% of the dye is fixed onto the fibre, and unfixed dyes are discharged in the spent dye-bath or in the wastewaters from subsequent washing operations [1]. Among the various colorants used in the textile industry, azo dyes are, nowadays, the most common compounds used for this purpose particularly ionic dyes applied in wool dyeing processes [2,3]. These compounds are characterized by the presence of one or more azo bonds (–N=N–), which are responsible for the colour and contribute partially for the recalcitrant nature of the textile effluents. Their resistance to biological degradation in classical activated sludge systems is well documented [4,5].

In order to meet the stringent levels of quality required for process water and wastewater treatment, membrane technologies have been object of special attention. Since the first experiments in 1990, several authors have showed the possibility of concentrating dyes, saving water, auxiliaries (mostly salts) and energy by the utilization of commercially available Nanofiltration (NF) membranes [6,7]. Nanofiltration has the advantage of retaining relatively small organic molecules and bivalent ions from water solutions, substances that are widely used in dyeing industry.

Most of the experiments reported in the literature have been performed in a wide range of dye concentrations and with mixtures of monovalent salts (NaCl) and reactive dyes. For instance, Koyuncu [7] found, in the presence of low salt concentrations (NaCl, 1 g/l), dye rejections greater than 98.5% for Reactive Black 5 (1–50 g/l) and greater than 99% for Reactive Orange 16 solutions in lower concentrations (0.1–5 g/l) with a NF membrane DS5 DK. Tang and Chen [8] obtained in average 98% dye removal in experiments carried out with Reactive Black 5 (0.09–1600 g/l) in the presence of NaCl (20 g/l) using a TFC-SR2 (Fluid Systems) NF mem-

* Corresponding author. Tel.: +351 275 319 759.
E-mail addresses: imscg@ubi.pt, imscg@yahoo.com (I.C. Gonçalves).

0376-7388/$ – see front matter © 2005 Elsevier B.V. All rights reserved.
doi:10.1016/j.memsci.2005.01.031

brane. In wool dyeing, residual dye bath concentrations are in general lower than 400 mg/l, thus studies on the nature and intensity of interactions solute–solute, solute–membrane at this range of concentration, may constitute a key factor on the feasibility of nanofiltration permeation processes [7–9]. The influence of those interactions on the membrane performance (selectivity and permeate flux) is, however, very dependent on the molecular size and concentration of dyes and salts, often leading to a high dye retentions due to steric and charge effects [1,7].

The success of the application of membranes for the purification of dyehouse wastewaters is related, among other factors, with the magnitude of the permeate fluxes decline. In nanofiltration, flux is affected by concentration polarization or by fouling phenomena. Either contributes for a decrease of the driving force for the filtration leading to an increase of the osmotic pressure or increase of the resistance to the flux due to adsorption, pore blocking or solute deposition [10].

In nanofiltration of dye solutions, various mechanisms have been presented as responsible for the decrease of flux values. Several authors have suggested a dynamic membrane formation as a direct result of the accumulation of dye molecules at the membrane surface. According to these researchers, this colloidal fouling layer, also caused by dye adsorption, could be removed by adequate membrane cleaning [7,8]. In reverse osmosis studies of dye–salt solutions, Al-Bastaki [11] refers the formation of a dynamic membrane originated by the concentrated dye at the membrane wall. However, the extend of dye adsorption as well as its reversibility are determined by factors such as dye-membrane physicochemical interactions (e.g., hydrophobic and polar interactions and charge transfer), which depend on the nature of the components, dye concentration, pH and cross-flow velocity.

In this paper, the effects of adsorption and osmotic pressure on the nanofiltration of a monoazo dye (C.I. Acid Orange 7) solution are investigated. Essays were carried out with a NF 45 membrane in different operational conditions, namely, pressure, cross-flow velocity and dye concentration.

1.1. Theory

The performance of pressure-driven membrane processes, namely nanofiltration, is associated to phenomena as concentration polarization and fouling caused by solute adsorption or pore blocking. Concentration polarization occurs due to the accumulation of solute that is being retained at the membrane interface. This results in a concentrated layer less permeable to the solvent associated to higher osmotic pressure ($\Delta\pi$) at the membrane interface which leads to a decrease of the effective driving force [10].

The traditional model for describing the concentration polarization (concentration profile) is based on the film theory that assumes a layer of concentrated solution with constant thickness, δ, adjacent to the membrane. A differential steady state mass balance for the solute leads, after integration in this layer, to the following equation [12]:

$$\frac{C_m - C_p}{C_f - C_p} = e^{\frac{J_v}{D/\delta}} \tag{1}$$

where J_v is the permeate (solvent) flux, D the solute diffusion coefficient, C_f, C_m and C_p are the solute concentration in the feed, at the membrane surface and in the permeate, respectively. The quantity D/δ represents the mass transfer coefficient, k, which depends on the kind of solute and equipment and is given by empirical correlations.

Due to the development of this concentration profile, two rejection coefficients are defined: the apparent rejection coefficient, f, and the intrinsic rejection coefficient f'. These two coefficients are related by the following equation [12,13]:

$$f' = \frac{f\, e^{\frac{J_v}{k}}}{1 - f\left(1 - e^{\frac{J_v}{k}}\right)} \tag{2}$$

The solute transport across the membrane is very often described by the solution-diffusion model that considers two main steps; sorption and diffusion.

In the diffusion step, the solute flux, J_s, is given by the first Fick's law, which after integration across a membrane of thickness l, from the solute concentration in the membrane side facing the feed, C'_m, to the solute concentration in the membrane side facing the permeate, C'_p, yields:

$$J_s = \frac{D_{sm}}{l}(C'_m - C'_p) \tag{3}$$

where D_{sm} is the diffusion coefficient of the solute in the membrane.

A sorption step describing the solute equilibrium between the membrane phase and the adjacent fluid phase is quantified by a partition coefficient, K_p. Taking into account that $K_p = \frac{C'_m}{C_m} = \frac{C'_p}{C_p}$, the following equation is obtained:

$$J_s = \frac{D_{sm} K_p}{l}(C_m - C_p) \tag{4}$$

where $\frac{D_{sm}K_p}{l}$ is the solute permeability coefficient and can be indicated by B.

Considering unhindered flow through the membrane, $J_s = J_v C_p$. Introducing this in Eq. (4) and using the definition of intrinsic rejection coefficient, the following expression is obtained:

$$f' = \frac{J_v}{J_v + B} \tag{5}$$

The solvent flux, J_v, is proportional to the effective applied pressure ($\Delta P - \Delta\pi$), as given in Eq. (6):

$$J_v = L'_p(\Delta P - \Delta\pi) \tag{6}$$

where ΔP is the applied pressure across the membrane, $\Delta\pi$ the osmotic pressure across the membrane and L'_p the solvent permeability coefficient.

The intrinsic rejection coefficient can then be written as:

$$f' = \frac{(L'_p/B)(\Delta P - \Delta\pi)}{(L'_p/B)(\Delta P - \Delta\pi) + 1} \quad (7)$$

The osmotic pressure can be calculated or experimentally determined. For very dilute solutions (concentrations lower than 0.2 mol/l) of a single solute, the calculation of the osmotic pressure can be made by the van't Hoff equation [14]. For higher concentrations, the osmotic pressure, π, can be given by [10,15,16]:

$$\pi = A_1 C + A_2 C^2 + A_3 C^3 + \cdots \quad (8)$$

where C is the solute concentration and A_1, A_2, and A_3 are the adjustable coefficients. In this work, nanofiltration experimental data are used to obtain a correlation of the osmotic pressure with the feed solute concentration [15,16].

When apparent rejection is sufficiently high, Eq. (1) can be written as $C_m = (C_f)\, e^{\frac{J_v}{k}}$ and the osmotic pressure difference can be calculated by the concentration at the membrane surface (C_m), as follows:

$$\Delta\pi = \pi(C_m) - \pi(C_p) \approx \pi(C_m) \quad (9)$$

since $\pi(C_p)$ is negligible.

In nanofiltration, besides the concentration polarization resistance, the solute(s)/membrane interactions may play an important role on the permeation performance due to adsorption effects that can be accounted for by an additional resistance, R_{ads}.

Permeate flux, J_v, can be predicted considering, besides osmotic pressure, a total resistance to flow, R_t, that is the sum of the intrinsic membrane resistance, R_m, and additional resistances like those caused by concentration polarization/gel formation, R_g, and R_{ads}. The permeate flux is given by [1]:

$$J_v = \frac{\Delta P - \Delta\pi}{\mu R_t} \quad (10)$$

where μ is the water viscosity and $R_t = R_m + R_g + R_{ads}$.

The permeability coefficient, L'_p, is defined as $1/\mu R_t$. The value of R_m is calculated from the pure water permeability coefficient, $L_p = 1/\mu R_m$.

2. Experimental

2.1. Membranes

The commercial membranes NF 45 from Filmtec were used. According to the manufacturer, these membranes are thin film composite on a polyester support viable for operation at pH from 2 to 10 and temperatures until 45 °C. The NF 45 membranes are reported in the literature as having a top layer of polyamide composition [17]. Polyamide compounds have amide and carboxyl groups bound to the aromatic rings, which tend to reduce membrane hydrophobicity (based on contact angle) [18]. Some authors reported that NF 45 displays an isoelectric point at pH 6.5 [19–21].

2.2. Nanofiltration experiments

Experiments were carried out in a plate and frame system LabUnit M20 (Danish Separation Systems AS-Denmark). A membrane effective surface area of 0.072 m^2 was used. Permeation experiments were run at constant temperature, 25 °C, with transmembrane pressures, ΔP, ranging from (6 to 36) $\times 10^5$ Pa (6 to 36 bar) and cross-flow velocities, $\langle u \rangle$, from 0.19 to 0.87 m/s (the maximum value reached by the recirculation pump).

Before the first permeation tests with model solutions, the membranes were pressurized at 42×10^5 Pa (42 bar) for about 3 h by recirculation of pure water. This procedure intends to minimize the influence of the compaction effects of the membrane in subsequent experiments.

The nanofiltration essays were performed in recycle mode, in which the retentate and permeate were both recycled back to the feed tank in order to hold the concentration of the feed solution constant. Samples of permeate and retentate were gathered for analyses. Sampling was done in steady state conditions (about 30 min after the last change of the parameters settings). Flow rates were monitored with the installed rotameters and manually by measuring the volume change with time. Measurements were done in triplicate. After each experiment, the membranes were carefully washed with pure water and a solution of an alkaline cleaning agent (P3 Ultrasil 11 from Henkel-Ecolab). Whenever the difference between the pure water permeability coefficients, measured before (L_p) and after (L'_p) permeation of dye solutions, was higher than 5%, a new set of membranes was used.

Solutions of a monoazo dye C.I. Acid Orange 7, AO7 (Fig. 1) in concentrations ranging from 2 to 2000 mg/l were used in the present work.

2.3. Reagents

The chemicals glycerol (with molecular weight, M, 92 Da), glucose (180 Da), sucrose (342 Da), raffinose (504 Da) and the polyethylenglycols (600, 1000 and 1500 Da) were supplied by Merck—Germany. Dyes Acid Orange 7, AO7 (351 Da), Acid Orange 33, AO33 (720 Da), Direct Red 80, DR80 (1356 Da) and sulfanilic acid (173 Da) were purchased from Sigma–Aldrich, USA. All the solutions were prepared with deionised water (conductivity less

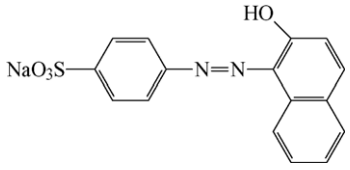

Fig. 1. Chemical structure of dye Acid Orange 7.

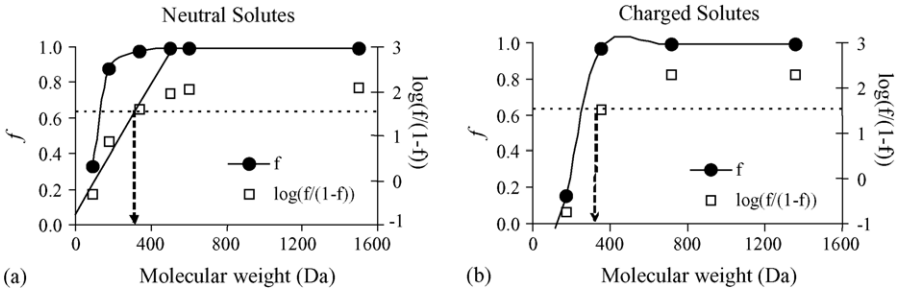

Fig. 2. The MWCO determination for NF 45 membrane for neutral (a) and charged (b) solutes.

than 1 μS/cm). These chemicals were used for the molecular weight cut-off determination and the dye AO7 in studies performed with NF45 membrane.

2.4. Analytical methods

Dye concentration was determined by spectrophotometry in a Perkin-Elmer spectrophotometer Lambda 6 (Perkin-Elmer, USA). These measurements were made at the maximum absorbance wavelength (λ_{max}) in the visible range. The conductivity measurements were performed at 25 °C with a Conductivimeter WTW, Tetra Cond—Germany. Total Organic Carbon, TOC, determinations were made in a Dohrmann Carbon Analyser DC-85 A (Dohramann, USA).

2.5. Membrane characterisation

The characterisation of the NF 45 membrane was performed by the determination of the pure water permeability coefficient, L_p, and the membrane molecular weight cut-off (MWCO).

The pure water permeate fluxes, J_w, were measured at ΔP of (10, 15, 20, 25, 30 and 35) $\times 10^5$ Pa (10, 15, 20, 25, 30 and 35 bar). The slope of the straight line J_w versus ΔP gives the pure water permeability coefficient, $L_p = (3.7 \times 10^{-5}$ kg/m^2 h Pa (3.7 kg/m^2 h bar).

The MWCO was determined from permeation experiments with solutions of organic charged solutes (ionic dyes from 350 to 1360 Da and precursors used in dye synthesis as sulfanilic acid) and organic neutral solutes (with molecular weights ranging from 92 to 1500 Da as glycerol, glucose, sucrose, raffinose and polyethylene glycol) at the operation conditions of $\Delta P = 1 \times 10^6$ Pa (10 bar) and $\langle u \rangle = 0.87$ m/s. The solute apparent rejection, f, is based on the TOC rejection of a 200 mg/l solution of each compound. The interception of the curve-fitting of the results of $\log(f/(1-f))$ versus solute M with the line of 97% rejection results in a MWCO of 340 Da for neutral solutes and 315 Da for charged solutes (Fig. 2) [22]. This slight difference could be attributed to electrostatic interactions between the membrane surface charge and the ionic components. However, as the experiments were performed near neutrality (pH 6, the isoelectric point of the membrane), only weak interactions are expected to occur.

3. Results and discussion

3.1. Flux decline

In order to develop a model to predict the flux decline and the rejection in nanofiltration of AO7 anionic dye solutions, two major factors were taken into account; osmotic pressure and adsorption.

The osmotic pressure of AO7 solutions was determined from the data of J_v versus ΔP, which are linearly correlated, for several concentrations. The extrapolation to zero flux, $J_v = 0$, yields the osmotic pressure, as this equals the value of the applied pressure ΔP, according to Eq. (6) [15,16]. As reported in the literature, the osmotic pressure values estimated by this method and those obtained experimentally by the vapour pressure method are in good agreement [16].

According to Eq. (8) the osmotic pressure values, π (Pa (atm)) are given by:

$$\pi = 0.62413C - 0.07433C^2 + 0.00299C^3 \quad (11)$$

For dye concentrations, C (g/l), higher than 3 g/l, the osmotic pressure becomes almost independent of the concentration (Fig. 3). This can be due to dye aggregation, which increases with concentration. As a consequence, a decrease in the number of particles in solution along with an increase of their size, lead to lower increments of $\Delta\pi$ with ΔC [23]. The values of $\pi(C_m)$ and of $\pi(C_p)$ obtained from Eq. (11) allow the calculation of $\Delta\pi$ (Eq. (9)).

The mass transfer coefficients, k, were obtained from the correlation proposed by Grober and used in LabUnit

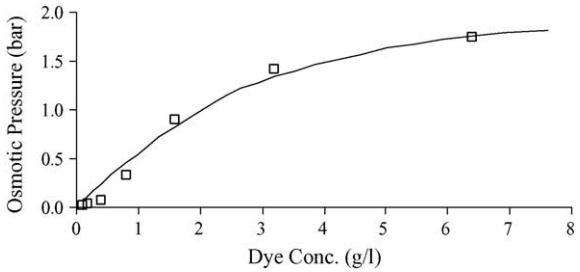

Fig. 3. Osmotic pressure of dye solutions in concentrations up to 7 g/l.

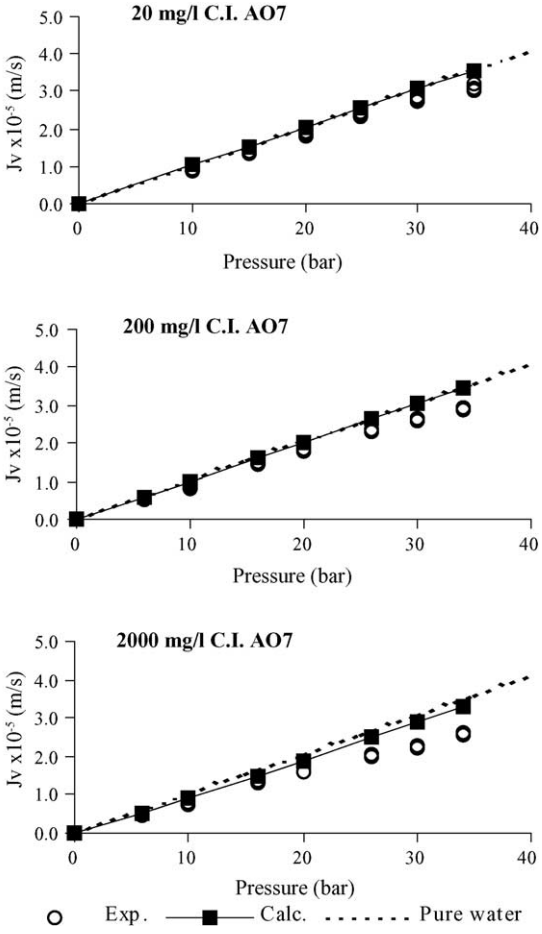

Fig. 4. Experimental (◯) and calculated (■) fluxes using the osmotic pressure model at feed dye concentrations of 20, 200 and 2000 mg/l.

M20 [24]:

$$Sh = 0.664\left(Re\frac{d_h}{L}\right)^{1/2} Sc^{1/3} \quad (12)$$

where d_h is the hydraulic diameter calculated as $4b$ (b is the channel semi-height) and L is the channel length. The Grober equation is an empirical correlation, but it can also be obtained from the boundary layer model that assumes an impermeable wall and low mass transfer rates. Geraldes et al. [25,26], have shown that the momentum boundary layer growth is independent of the permeation fluxes in the range of interest of nanofiltration (0.2×10^{-5} m/s $< J_v < 3 \times 10^{-5}$ m/s). Therefore, those assumptions do not influence the hydrodynamics boundary layer, and Eq. (12) can then be applied for the range of the permeation velocities in nanofiltration systems.

The nanofiltration permeation performance is assessed in Fig. 4, which shows the variation of J_v versus ΔP, at different feed dye concentrations. The deviation of the experimental results from those calculated by the equation $J_v = L_p(\Delta P - \Delta\pi)$, where L_p is the pure water permeability coefficient and $\Delta\pi$ is calculated by Eqs. (9) and (11), increases with dye concentration. The flux decline ($\Delta J_v = J_v - J_w$) increased from 0.3190×10^{-5} m/s for a dye concentration of 20 mg/l to 0.8117×10^{-5} m/s for a dye concentration of 2000 mg/l (in experiments run at ΔP of 30×10^5 Pa (30 bar), 25 °C and cross-flow velocity of 0.87 m/s).

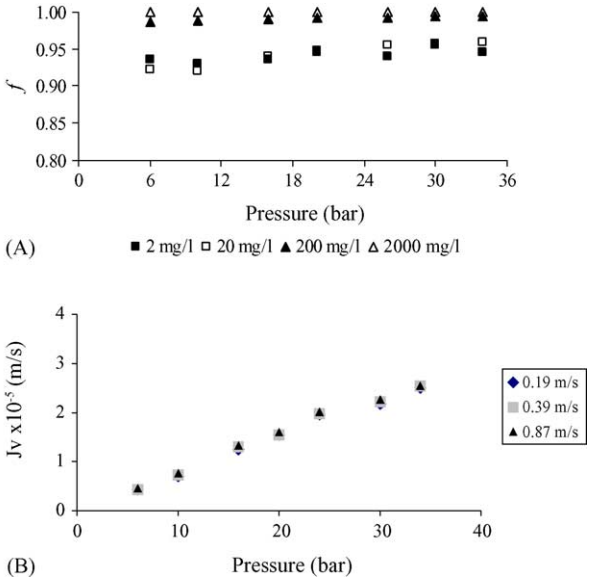

Fig. 5. Variation of apparent rejection, f, and permeate fluxes, J_v, with pressure: apparent rejections obtained at several feed dye concentrations of essays performed at maximum cross-flow velocity, $\langle u \rangle = 0.87$ m/s (A). Permeate fluxes for a feed dye concentration of 2000 mg/l at different cross-flow velocities (B).

From the data of permeate fluxes, J_v, and apparent rejection, f, as functions of ΔP obtained at different circulation velocities, $\langle u \rangle$, it was observed that both are independent of $\langle u \rangle$ (Fig. 5). Therefore, the concentration polarization resistance is not contributing in a significant way to the flux decline. The total resistance to permeation, R_t, is then attributed mainly to the membrane itself and to the adsorption effects.

The intrinsic membrane resistance, R_m, was calculated from the slope of the linear plot of J_w versus ΔP. A value of 1.1×10^{14} m^{-1} for R_m was obtained. The adsorption resistance, R_{ads}, was evaluated from the comparison of permeate fluxes before (J_w) and after (J_w^*) dye permeation. These results are shown in Table 1. Also a flux decline with time was observed for a dye solution of 350 mg/l, as shown in Table 2.

Table 1
Ratio between the water flux measured before (J_w) and after (J_w^*) running experiments

Dye concentration (mg/l)	J_w^*/J_w
2	0.977
20	0.970
45	0.967
180	0.962
200	0.960
450	0.954
880	0.950
2000	0.947

Table 2
Permeate flux along time of a 350 mg/l dye solution at pH 6.5 (operational conditions: $\Delta P = 16 \times 10^5$ Pa (16 bar), $T = 25\,^{\circ}$C, $\langle u \rangle = 0.87$ m/s)

Elapsed time (h)	J_v ($\times 10^{-5}$ m/s)
0.5	1.919
1.0	1.908
3.0	1.860
6.0	1.852
9.0	1.829
12.0	1.828

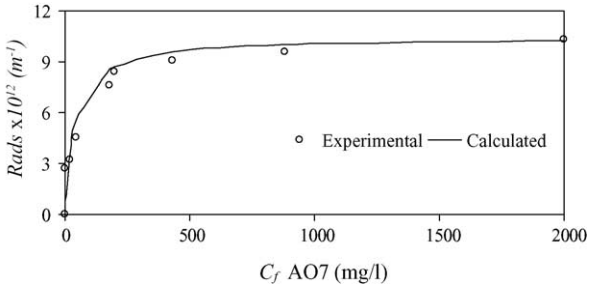

Fig. 6. Adsorption resistances (R_{ads}) for feed dye solutions (C_f) ranging from 2 to 2000 mg/l and curve fitting on the basis of Langmuir isotherm type curves.

During the permeation of dye solutions, the adsorption of dye molecules at the membrane surface and inside the pores contributes to the decrease of the membrane pore sizes and as a consequence to the alteration of the pure water permeability coefficient, L_p. Then a new coefficient L'_p was determined from the slope of the straight line obtained from the experimental data of J^*_w versus ΔP. These results are indicated in Table 3. The L'_p coefficient was shown to be a function of C_f according to the results given in Table 3, therefore the adsorption resistance, R_{ads}, is also a function of C_f, and is considered independent of pressure. As data suggest R_{ads} and C_f can be correlated in the form of a Langmuir type isotherm.

Assuming that R_{ads}, is proportional to the amount of dye sorbed per unit surface area, q (or to the fraction of covered surface, θ) and considering that in the Langmuir equation q is related to the equilibrium concentration, C [14]:

$$\theta = \frac{q}{q_{max}} = \frac{bC}{1 + bC} \tag{13}$$

a similar relationship between $R_{ads} \times 10^{12}$ (m^{-1}) and the feed dye concentration, C_f (mg/l) could thus be written as:

$$R_{ads} = \frac{R_{max} b C_f}{1 + bC_f} \tag{14}$$

where b (0.025 l/mg) and R_{max} (10.45 m^{-1}) are adjustable parameters. The former is related to the adsorbate–adsorbent affinity and the latter to the maximum adsorbate (solute) binding capacity. As shown in Fig. 6, a good fit was obtained. As dye concentration increases, R_{ads} increases and tends to a plateau, as postulated by the Langmuir isotherm. A saturation value of R_{ads} (associated to R_{max} in Eq. (14)) is expected to be attained which is probably influenced by the dye–dye aggregation mechanisms [2].

Dye molecules have amino, sulphonic and hydroxyl groups as substituents bound to the aromatic rings. Those functional groups could interact with the membrane that has also functional groups as carboxyl, amide and amino [17,19–21]. The adsorption mechanism could be based on multiple interactions such as electrostatic, hydrophobic, van der Waals and hydrogen bonds. At its isoelectric point, the membrane is likely to present non-ionised acid and basic groups, and so the uptake of anionic dyes is lower. Although experiments were performed near the isoelectric point (pH 6–6.5) [19,21] where electrostatic forces are minimized, another type of forces could take place, like those contributing to dye aggregation (e.g., van der Waals forces, in the particular case of dye AO7) that in turn enhance the efficiency of the adsorption process (in a single site two or more molecules can then be bound). Aggregation increases with dye concentration and ionic strength [2,23].

Including R_{ads} in Eq. (10) the permeate fluxes, J_v, were then calculated. As shown in Fig. 7 experimental and calculated values agree quite well, corroborating the idea that the deviations shown in Fig. 4 are due to the fact that the resistance caused by adsorption should be taken into account, although a small discrepancy is still observed at high pressures and high dye concentrations (2000 mg/l).

Table 3
Values of the solvent permeability coefficient, L'_p and adsorption resistance, R_{ads}, obtained at several feed dye concentrations, C_f

C_f (mg/l)	L'_p (kg/(m^2 h Pa) kg/(m^2 h bar))	R_{ads} ($\times 10^{12}$ m^{-1})
0	3.69	0.00
2	3.43	2.71
20	3.29	3.24
45	3.25	4.39
180	3.17	7.45
200	3.16.	8.28
433	3.09	8.97
880	3.00	9.48
2000	2.76	10.20

3.2. Variation of rejection coefficients with concentration

The experimental data displayed in Fig. 5 show an increase of the apparent rejection coefficient with the dye concentration. Adsorption effects can explain not only the increase of the total resistance to the permeation fluxes but also the increase of the rejection coefficients with concentration.

According to the solution-diffusion model and specifically to Eq. (5) the intrinsic rejection coefficient of the solute, f',

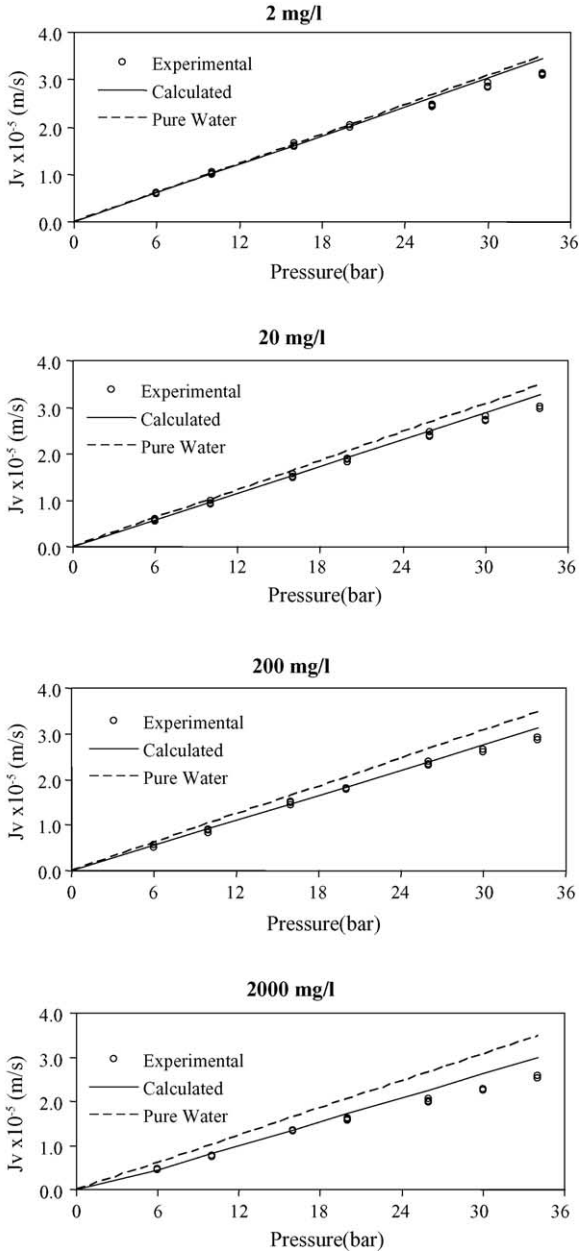

Fig. 7. Experimental (◯) and calculated fluxes (—) given by the resistance-in-series model.

is a function of the solvent flux, J_v, and of the solute coefficient permeability, B. From the experimental values of J_v and C_p and using Eq. (1) to calculate C_m, the B coefficients were calculated from Eq. (4) and correlated with feed dye concentration, C_f, as follows:

$$B = 0.473^{*} C_f^{-0.738} \tag{15}$$

The intrinsic rejection coefficients could then be calculated by the solution-diffusion model by means of Eqs. (5), (6) and (7). Those values are compared with the experimental f' obtained from the definition equation $\left(f' = \frac{C_m - C_p}{C}\right)$,

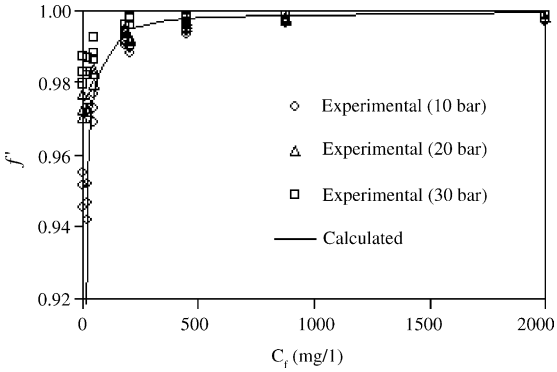

Fig. 8. Intrinsic rejection coefficient, f', as a function of the feed dye concentration, C_f, at pressures of (10, 20 and 30) $\times 10^5$ Pa (10, 20 and 30 bar).

where C_m was obtained from Eq. (1) with the experimental values of C_f, J_v and C_p. As can be observed in Fig. 8 those experimental and calculated values are in good agreement. For the intrinsic rejection coefficient as function of C_f, a Langmuir isotherm type curve was then fitted as follows:

$$f'_{calc} = \frac{b' C_f}{1 + b' C_f} \tag{16}$$

where b' is a coefficient with the value of 0.9843 l/mg. The data were obtained at ΔP of (10, 20 and 30) $\times 10^5$ Pa (10, 20 and 30 bar), bearing in mind the applied pressure did not show a significant effect on the intrinsic rejection coefficient.

4. Conclusions

The productivity and selectivity of the membrane remained quite high during the nanofiltration of dye solutions. Adsorption was found to be the main phenomenon contributing to the total resistance and thus it can explain the solvent flux decline. The results obtained for permeate flux show that the resistance-in-series model agrees closely with the experimental data. Also, in predicting intrinsic rejections coefficients, f', as function of feed dye concentration, C_f, it was clearly found that adsorption affects not only the solvent permeability coefficient but also the solute permeability coefficient (B), resulting in a Langmuir isotherm type curve for f' versus C_f.

It should be emphasized that observed flux decline was not significant for the range of dye concentrations studied (ΔJ_v of 26.5% relatively to pure water for a dye concentration of 2000 mg/l at 20×10^5 Pa (20 bar)). As residual dye concentrations in wool dyeing effluents are lower (between 30 and 50 mg/l, depending on the shade) [9], its removal seems not to be a problem. Furthermore, the high rejections obtained (higher than 95% at a pH 6–7) corroborate the idea that this technology could give a good contribution for the elimination of those recalcitrant compounds from the environment.

Nomenclature

A_1, A_2, A_3	coefficients (Eq. (8))
b	coefficient of a type Langmuir equation (l/mg)
b'	experimental coefficient (l/mg)
B	solute permeability coefficient (m/s)
C	solute concentration (mg/l)
C_f	feed solute concentration (mg/l)
C_m	solute concentration at the membrane surface (mg/l)
C'_m	solute concentration in the membrane side facing the feed (mg/l)
C_p	solute concentration in the permeate (mg/l)
C'_p	solute concentration in the membrane side facing the permeate (mg/l)
d_h	hydraulic diameter (m)
D	solute diffusion coefficient (m^2/s)
D_{sm}	solute diffusion coefficient in the membrane (m^2/s)
f	apparent rejection coefficient, defined by $f = (C_f - C_p)/C_f$
f'	intrinsic rejection coefficient, defined by $f' = (C_m - C_p)/C_m$
J_v	solvent volumetric flux (m/s)
J_w	pure water permeation flux, defined by $J_w = L_p \Delta P$ (m/s)
J_w^*	pure water permeation flux after the experiments (m/s)
k	mass transfer coefficient (m/s)
K_p	partition coefficient
l	membrane thickness (m)
L	channel length (m)
L_p	pure water permeability coefficient, defined by $L_p = 1/(\mu R_m)$ (m/s; kg/m^2 h Pa (kg/m^2 h bar))
L'_p	solvent permeability coefficient, defined by $L'_p = 1/(\mu R_t)$ (m/s; kg/m^2 h Pa (kg/m^2 h bar))
M	molecular weight (Da)
MWCO	molecular weight cut-off (Da)
P	pressure (bar)
ΔP	transmembrane pressure (bar)
q	amount of dye sorbed per unit surface membrane area (g/m^2)
q_{max}	maximum amount of dye sorbed per unit surface membrane area (g/m^2)
R_{ads}	adsorption resistance (m^{-1})
R_g	concentration polarization/gel layer formation resistance (m^{-1})
R_m	membrane resistance (m^{-1})
R_{max}	maximum adsorption resistance (m^{-1})
R_t	total resistance (m^{-1})
Re	Reynolds number (dimensionless)
Sc	Schmidt number (dimensionless)
Sh	Sherwood number (dimensionless)
$\langle u \rangle$	cross-flow velocity (m/s)

Greek symbols

δ	polarization layer thickness (m)
θ	fraction of membrane surface covered
μ	water viscosity (Pa s)
π	osmotic pressure (Pa (bar; atm))
$\Delta\pi$	osmotic pressure difference (Pa (bar; atm))

References

[1] R. Jiraratananon, A. Sungpet, P. Luangsowan, Performance evaluation of nanofiltration membranes for treatment of effluents containing reactive dye and salt, Desalination 130 (2000) 177–183.

[2] H. Zollinger, Color Chemistry, second ed., VCH, Weinheim, 1991.

[3] C.M. Carliell, S.J. Barclay, N. Naidoo, C.A. Buckley, D.A. Mulholland, E. Senior, Microbial decolourisation of a reactive azo dye under anaerobic conditions, Water SA 21 (1995) 61–69.

[4] J.A. Field, Limits of anaerobic biodegradation, Water Sci. Technol. 45 (10) (2002) 9–18.

[5] D. Méndez-Paz, F. Omil, J.M. Lema, Modeling of the Acid Orange 7 anaerobic biodegradation, Water Sci. Technol. 48 (6) (2003) 133–139.

[6] J. Sójka-Ledakowicz, T. Koprowski, W. Machowki, H.H. Knudsen, Membrane filtration of textile dyehouse wastewater for technological water reuse, Desalination 119 (1998) 1–10.

[7] I. Koyuncu, Reactive dye removal in dye/salt mixtures by nanofiltration membranes containing vinylsulphone dyes: effects of feed concentration and cross-flow velocity, Desalination 143 (2002) 243–253.

[8] C. Tang, V. Chen, Nanofiltration of textile wastewaters for water reuse, Desalination 143 (2002) 11–20.

[9] I.G. Laing, The impact of effluent regulations on the dyeing industry, Rev. Prog. Colorat. 21 (1991) 56–71.

[10] H. Nabetani, M. Nakajima, A. Watanabe, S. Nokao, S. Kimura, Effects of osmotic pressure and adsorption on ultrafiltration of ovalbumin, AIChE J. 36 (6) (1990) 907–915.

[11] N. Al-Bastaki, Removal of methyl orange dye and Na_2SO_4 salt from synthetic waste water using reverse osmosis, Chem. Eng. Process. 43 (12) (2004) 1561–1567.

[12] M. Mulder, Basic Principles of Membrane Technology, second ed., Kluwer Academic Publishers, Boston, 1996.

[13] P. Aptel, M. Clifton, Ultrafiltration in synthetic membranes: science engineering and applications, in: P.M. Bungay, A.A. Lonsdale, M.N. de Pinho (Eds.), NATO AST Series C, 181, D. Reidel Publishing Company, Holland, 1986, pp. 249–305.

[14] I.N. Levine, Physical Chemistry, fifth ed., McGraw Hill International Edition, 2002.

[15] H. Nabetani, M. Nakajima, A. Watanabe, Development of a new type of membrane osmometer, J. Chem. Eng. Jpn. 25 (3) (1992) 269–274.

[16] V. Geraldes, V. Semião, M.N. de Pinho, Flow and mass transfer modelling of nanofiltration, J. Membr. Sci. 191 (2001) 109–128.

[17] B. Van der Bruggen, C. Vandecasteele, Flux decline during nanofiltration of organic components in aqueous solution, Environ. Sci. Technol. 35 (2001) 3535–3540.

[18] J. Cho, G. Amy, J. Pellegrino, Membrane filtration of natural organic matter: initial comparison of rejection and flux decline characteristics with ultrafiltration and nanofiltration membranes, Water Res. 33 (11) (1999) 2517–2526.

[19] T. Courtois, Characterization des membranes de nanofiltration, First Nanofiltration and Application Workshop, France–Canada, Trois-Revières, 2–4 Juin 1997.
[20] Y. Xu, R.E. Lebrun, Investigation on the solute separation by charged nanofiltration membrane: effect of pH, ionic strength and solute type, Desalination 158 (1999) 93–104.
[21] X.L. Wang, W.N. Wang, D.X. Wang, Experimental investigation on separation performance of nanofiltration membranes for inorganic electrolyte solutions, Desalination 145 (2002) 115–122.
[22] M.J.F. Rosa, Selective separation of organic compounds from aqueous streams by ultrafiltration and nanofiltration, Ph.D. Thesis, IST, Technical University of Lisbon, 1995.
[23] S. Bracko, J. Span, Osmotic coefficients of C.I. Acid Orange 7 in aqueous solution and in the presence of simple electrolyte, Dyes Pigments 35 (2) (1997) 165–169.
[24] R.F. Madsen, Hiperfiltration and Ultrafiltration in Plate-and-Frame Systems, third ed., Elsevier, 1989.
[25] V. Geraldes, V. Semião, M.N. de Pinho, Nanofiltration mass transfer at the entrance region of a slit laminar flow, Ind. Eng. Chem. Res. 37 (12) (1998) 4792–4800.
[26] V. Geraldes, V. Semião, M.N. de Pinho, The effect on mass transfer of momentum and concentration boundary layers at the entrance region of a slit with a nanofiltration membrane wall, Chem. Eng. Sci. 57 (2002) 735–748.